PHYSICAL REVIEW B **81**, 094412 (2010)

Magnetic aftereffect in compressively strained GaMnAs studied using Kerr microscopy

L. Herrera Diez,* J. Honolka, and K. Kern
Max-Planck-Institut für Festkörperforschung, Heisenbergstrasse 1, 70569 Stuttgart, Germany

H. Kronmüller
Max-Planck-Institut für Metallforschung, Heisenbergstrasse 3, 70569 Stuttgart, Germany

E. Placidi and F. Arciprete
Dipartimento di Fisica, CNR-INFM, Università di Roma "Tor Vergata," Via della Ricerca Scientifica 1, I-00133 Roma, Italy

A. W. Rushforth, R. P. Campion, and B. L. Gallagher
School of Physics and Astronomy, University of Nottingham, University Park, Nottingham NG7 2RD, United Kingdom
(Received 5 October 2009; revised manuscript received 12 February 2010; published 11 March 2010)

We study the magnetic aftereffect in compressively strained GaMnAs by means of Kerr microscopy. Under constant magnetic field conditions, a dramatic decrease in domain-wall velocity with time is observed, which is attributed to the irreversible magnetic aftereffect. The time- and space-resolved dynamics of single domain walls are used to derive the time dependence of the magnetization that is modeled considering two coexisting relaxation processes on fast and slow time scales. From fitting of the magnetization vs time curves, the activation volumes for two different GaMnAs samples have been estimated.

DOI: 10.1103/PhysRevB.81.094412 PACS number(s): 75.50.Pp, 75.60.Ch, 75.60.Jk, 75.60.Lr

The ferromagnetic semiconductor GaMnAs (Ref. 1) has been shown to be an excellent model system for the up-and-coming combination of semiconductor electronics and magnetism.[2] In connection with practical applications, magnetic aftereffects[3] are often studied in materials used for magnetic-recording media where the time stability of magnetization is of crucial importance.[4,5] Studies in the literature present the observation of the magnetic aftereffect in both compressively[6] and tensile[7] strained GaMnAs. However, a detailed analysis of this magnetic relaxation process in a diluted magnetic semiconductor is still to be done and is the motivation for the present work.

Relaxation effects during domain-wall transitions as described by Néel[3,8] have two distinct origins and are called reversible and irreversible aftereffects. In the irreversible aftereffect, the time variation in the magnetization is attributed to the thermal activation of the magnetization reversal. The reversible aftereffect (or diffusion aftereffect) is also a thermally activated process but it is associated to the diffusion and reorientation of the symmetry axis of point defects inside the structure of the ferromagnet.[9,10] This diffusion of defects is a consequence of the general tendency of the system to find a lower-energy minimum. In this case, a new lower minimum can be found by changing the orientation of the symmetry axis of the defect with respect to the local magnetization direction within the domain wall. The most effective path to realize this is a short-range migration to a different neighboring site. This lower-energy minimum can only be found if the symmetry of the defect (interstitial) sites differs from that of the ideal lattice (substitutional) sites.[11,12]

Although GaMnAs seems to be a good candidate to show the reversible aftereffect due to the well-known presence of interstitial Mn atoms in the lattice,[13] the symmetry of interstitial and substitutional sites prevent it. In GaMnAs, the interstitial sites can have either tetrahedral or hexagonal symmetry, however, from experimental and theoretical work, it is known that interstitial Mn atoms exclusively occupy tetrahedral sites.[14,15] As previously mentioned, this has important consequences for the magnetic aftereffect. Since the nonequality of the symmetry of the interstitial sites with respect to the substitutional sites is not fulfilled in GaMnAs (both sites are tetrahedral), the reversible aftereffect is not expected. Therefore, taking into account these symmetry considerations, we attribute the relaxation processes observed in this study to the irreversible aftereffect.

Viscosity measurements have been carried out on two samples grown in two different molecular-beam epitaxy laboratories to confirm that the present study on the magnetic aftereffect has a far-reaching validity in the field of ferromagnetic GaMnAs materials. The as-grown samples employed in this study (samples A and B, respectively) have different Mn concentrations (2.5% and 8% Mn) and Curie temperatures (53 and 65 K) and are also of different thicknesses (170 and 50 nm). Details of the growth procedure of samples A and B can be found elsewhere.[16–18]

We reveal the irreversible magnetic aftereffect in compressively strained GaMnAs by tracking the position of individual domain walls versus time. The respective position is monitored in movies taken during Kerr microscopy.[19] To obtain a well-defined initial magnetization state, the magnetic film was first saturated in a positive field of 500 Oe. After reducing the field to zero in one step, an opposing magnetic field of a certain value was applied that remained constant through the time of the Kerr microscopy measurement. All measurements were carried out at a temperature of 3 K and with the magnetic field applied along the uniaxial easy axis direction ($[110]$ and $[1\bar{1}0]$ for samples A and B, respectively).

The time variation in the position of the domain wall is tracked as a function of the applied magnetic field and always in the exact same section of the film. The starting time

 ©2010 The American Physical Society

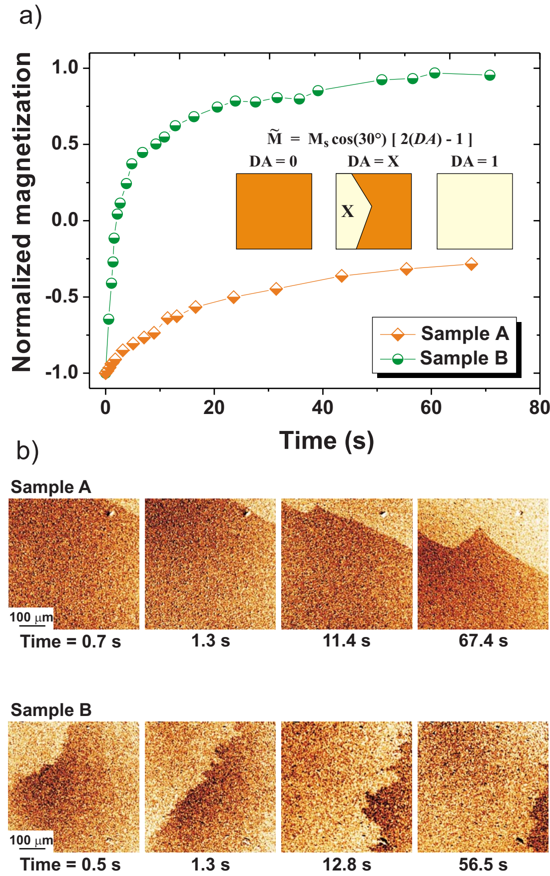

FIG. 1. (Color online) (a) Normalized magnetization vs time for samples A (diamonds) and B (circles) at a constant magnetic field of 28.0 Oe and 24.6 Oe, respectively. The derivation of the magnetization values from the domain area (DA) at a given time is also schematized. (b) Kerr microscopy images corresponding to the curves in (a) for samples A (top) and B (bottom) at the indicated times.

of the measurement ($t=0$) is considered to be the time corresponding to the frame (in the Kerr microscopy movie) that precedes the first image where the smallest switched area is observed. The reverse domain area (DA) at different times is normalized with respect to the size of the whole image ($500\ \mu\text{m} \times 500\ \mu\text{m}$) and by considering the difference between the switched and the unswitched areas, a local value of the magnetization ($\tilde{M}$) for the portion of material under analysis can be evaluated. This calculation is schematized in Fig. 1(a) where M_s is the saturation magnetization of the film obtained from superconducting quantum interference device magnetometry. The corresponding saturation magnetization values for samples A and B are 10 emu/cm^3 and 40 emu/cm^3, respectively. In the following, the magnetization values used in the calculations of the magnetic aftereffect will correspond to $\tilde{M}$.

In-plane magnetized GaMnAs/GaAs materials with Curie temperatures and magnetization values in the range of those corresponding to the samples studied here are known to exhibit a biaxial anisotropy landscape at low temperatures that evolves into an uniaxial regime at higher temperatures.[20–23] The angle between the global easy directions and the biaxial and uniaxial easy axes is a material- and temperature-dependent property. While for sample A, we have shown that the global easy axes are located approximately $\phi=30°$ away from the uniaxial easy axis along [110] (Ref. 16) and for sample B, the global easy direction is at $\phi=45°$ with respect to the uniaxial easy axis ($[1\bar{1}0]$). Since the magnetic field is applied along the uniaxial easy axis, the value of the projection of the magnetization on the direction of the applied field for the initial state (magnetization in zero field after saturation) is approximately $-M_s \cos(30°)$ for sample A and $-M_s \cos(45°)$ for sample B and with domain-wall displacement (120° and 90° domain wall, respectively) this value can grow up to $M_s \cos(30°)$ and $M_s \cos(45°)$, respectively, for the switched state. Therefore, for the areas occupied by the reverse domains, the change in magnetization is $\Delta M = 2M_s \cos(30°)$ for sample A and $\Delta M = 2M_s \cos(45°)$ for sample B with respect to the initial state. We consider Stoner rotation processes negligible in the present case since the applied magnetic fields are very low. Only at much higher fields, the magnetization would further rotate in a coherent way.

A typical curve of normalized magnetization vs time calculated in the described manner [and divided by $M_s \cos(30°)$ and $M_s \cos(45°)$ for normalization] is presented in Fig. 1(a) for samples A and B at a constant magnetic field of 28.0 Oe and 24.6 Oe, respectively. We observe that the slope of these curves, namely, the domain-wall velocity, decreases dramatically as a function of time which is a signature of the magnetic aftereffect.

The Kerr microscopy images in Fig. 1(b) correspond to four points of the curves in Fig. 1(a) for samples A (top) and B (bottom) taken at the indicated times. On a larger scale, the domain is mainly moving in one direction, however, kinks in the wall shape are observed which we attribute to infrequent strong pinning events at large domain-wall pinning centers (macropins). These stronger pinning events introduce inhomogeneous variations in the domain-wall velocity on a local scale.

It remains to verify that the observed time dependence of the domain-wall velocity is not an artifact due to the influence of light penetrating the sample during the acquisition of the Kerr microscopy movies. From the time-dependent magnetotransport measurements shown in the following, it becomes evident that the aftereffect is also visible in the absence of the Kerr microscope illumination. The Hall-bar structures employed for these measurements are of 100 μm width and fabricated by photolithography. The 90° orientation of the Hall-bar longitudinal axis with respect to the direction of the magnetic field favors the nucleation of magnetic domains at the sides of the Hall bars.[22] This also allows for the investigation of the aftereffect in a magnetization reversal involving more than one domain.

The time and the magnetic field dependence of the planar Hall voltage of sample B are presented in Fig. 2 (left) and (right), respectively. The time dependence is again recorded under constant magnetic field conditions with fields of 33.4 Oe (bottom), and 33.9, 34.0, and 39.6 Oe (top). The decrease in domain-wall velocity over time observed in the single domain case (Fig. 1) is also evident in the overall magne-

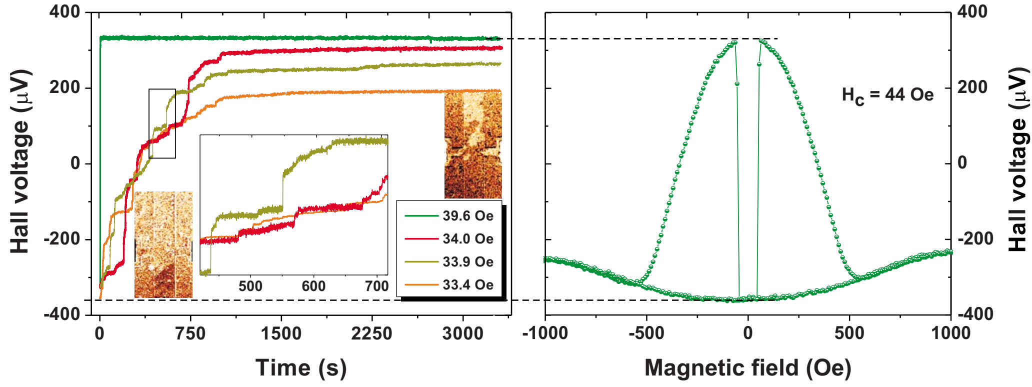

FIG. 2. (Color online) (Left) Planar Hall voltage vs time for sample B at different constant values of the magnetic field: 33.4 Oe (bottom), and 33.9, 34.0, and 39.6 Oe (top). The steps observed in all the curves (see inset) correspond to the growth of single magnetic domains. (Right) Planar Hall voltage as a function of magnetic field.

totransport signal from $t=0$ to 3300 s. Moreover, looking more closely to the time dependence of the planar Hall voltage, small steps corresponding to the displacement of single domain walls after nucleation can be observed. In the inset of Fig. 2 (left), a few of these small steps are shown in more detail. The shape of the magnetoresistive signal of a single step strongly resembles those shown in Fig. 1(a) for the time dependence of the domain size for a single domain process, suggesting a similar dynamics. However, it is important to mention that in a multidomain configuration, other contributions to the domain-wall dynamics may arise with respect to the single domain scenario. Interactions between neighboring domain walls can influence the dynamics by including affinities between neighboring Néel walls.[24] At the same time, pinning effects at the Hall-bar edges can play a role. Two typical Kerr images of the Hall device during magnetotransport are shown in Fig. 2, one in the early stage of reversal (left) and the other approximately 1 h after applying a constant magnetic field (right). For comparison on the right side of Fig. 2, the planar Hall voltage vs magnetic field is shown while sweeping the magnetic field between ± 1000 Oe representing a full magnetization reversal of the entire device. The full domain-wall transition at $H_c = \pm 44$ Oe switches the device between two well-defined magnetoresistive states corresponding to $\approx \pm 325$ mV, and the time-dependent graphs in Fig. 2(a) can be compared to these values.

In the following, the results of domain size vs time for samples A and B will be analyzed in terms of the known models describing the magnetic aftereffect.

I. MODELING OF THE MAGNETIC AFTEREFFECT

The description of the magnetic aftereffect involves deriving an expression for the time dependence of the magnetization $M(t)$. This can be done in a simple way by considering the effect as a relaxation process with a relaxation time τ,[25,26]

$$M(t) = \alpha + \beta \exp[-t/\tau]. \tag{1}$$

The constants α and β are time independent and the relaxation time τ, for the case where the transition occurs via domain-wall motion, depends both on temperature and magnetic field according to[26,27]

$$\tau = \tau_0 \exp[E_A/k_B T]. \tag{2}$$

Here τ_0 is a pre-exponential factor fairly independent of the field, T is the temperature, and E_A is the activation energy that has the following expression:

$$E_A = 2M_s \cos(\phi) V (H_A - H), \tag{3}$$

where V is the activation volume, $2M_s \cos(\phi)$ is the total magnetization change during the switching process projected on the field direction, and H_A is the propagation field without thermal activation. In a more complex scenario where a wide distribution of relaxation times are present, the following expression is commonly used assuming a flat-topped distribution function for τ:

$$M(t) = \gamma - S \ln[t], \tag{4}$$

where S is the coefficient of magnetic viscosity that includes the activation volume.[25]

In the present study, the best fitting of the time dependence of the magnetization is obtained neither considering a single relaxation process nor a flat-topped distribution of relaxation times. This disagreement with the Néel formulation has also been reported in studies analyzing the relaxation of the thermoremanent magnetization in GaMnAs within the cluster/matrix model[28] and in other materials such as manganite compounds. In the latter case, the time dependence of the magnetization is well described by a stretched exponential function but also by a model with an exponential and a logarithmic term which the authors suggest may be due to the existence of two relaxation processes acting in series.[29]

The stretched exponential function can also fit our experimental data, however, a model considering two relaxation processes gives an equally satisfying result. The fittings shown in Fig. 3 correspond to the combination of two distinct relaxation processes of the form of Eq. (1) with relaxation times τ_1 and τ_2. The first relaxation time describes the fast increase in $M(t)$ at short time scales while τ_2 covers the slow increase for $t \gg \tau_1$.

Small contributions from other relaxation processes cannot be excluded but from the good agreement between fit and data, we conclude the aftereffect is dominated by two main relaxation processes.

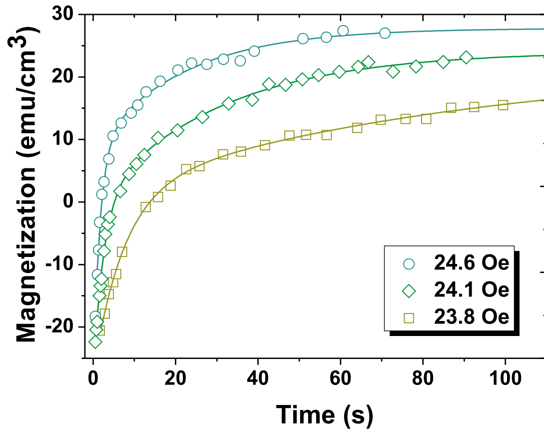

FIG. 3. (Color online) Magnetization ($\widetilde{M}$) vs time plots (sample B) for different values (23.8, 24.1, and 24.6 Oe) of the applied magnetic field and the corresponding fit curves (solid lines). The fitting was done considering two coexisting relaxation processes each one described by Eq. (1) with relaxation times τ_1 and τ_2.

According to Eqs. (2) and (3), the activation volume can be derived from the magnetic field dependence of the relaxation time at a given temperature. The logarithm of the relaxation times $\tau_1(H)$ and $\tau_2(H)$ plotted in Figs. 4(a) and 4(b) (for samples A and B, respectively) were extracted from fittings shown in Fig. 3 for sample A and from those corresponding to sample B.

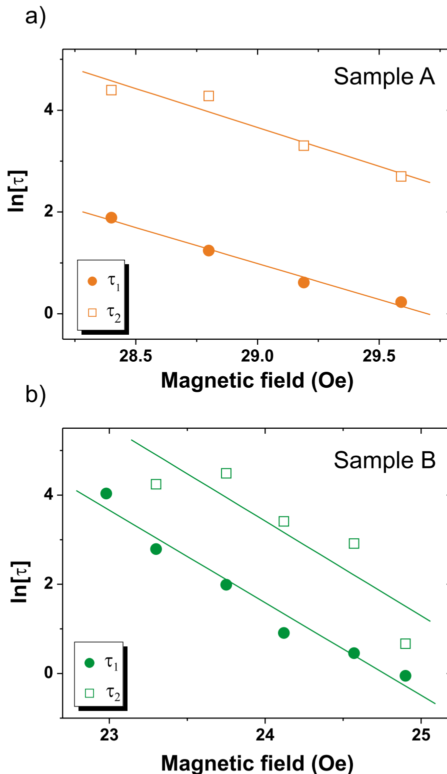

FIG. 4. (Color online) Linear dependence of $\ln[\tau(s)]$ vs magnetic field for τ_1 (circles) and τ_2 (squares) [(a) sample A and (b) sample B], the corresponding linear fittings of the data points are shown in solid lines.

At this point we want to shortly comment on the possibility to derive the activation volume also from the temperature dependence of the relaxation time in Eq. (2), a method often found in the literature.[30] This method is not applicable in the case of GaMnAs in which the anisotropy energy and saturation magnetization are strongly temperature dependent. In fact, we would expect a temperature-dependent activation volume due to the strong changes in the magnetic anisotropy. In contrast, by measuring the magnetic field dependence of τ at a single temperature of 3 K as shown in this work, we keep most of the magnetic quantities in Eq. (2) constant. In Fig. 4, the slope of the curves of $\ln[\tau_1]$ and $\ln[\tau_2]$ vs magnetic field is then equal to $2M_S \cos(\phi)V/k_BT$ from which the activation volume can be estimated. From the field dependence of τ_1, volumes $V_{A1}=(3.4\pm 0.2)\times 10^4$ nm^3 for sample A and $V_{B1}=(1.5\pm 0.1)\times 10^4$ nm^3 for sample B are obtained. From the plot of $\ln[\tau_2]$, we get $V_{A2}=(3.7\pm 0.7)\times 10^4$ nm^3 and $V_{B2}=(1.6\pm 0.4)\times 10^4$ nm^3 for samples A and B, respectively. Comparing these values to the literature, we find that activation volumes of similar size are found in magnetic-recording materials such as barium ferrite films.[31]

Activation volumes calculated from aftereffect measurements are related to the energy barrier involved in the first elementary magnetization reversal.[32] The activation volume is the volume of material that changes magnetization as the result of going from a maximum (activated state) to a local minimum-energy state by a change in the position of the domain wall. This volume is often not only related to this elementary magnetization reversal but also to the entire volume swept by the domain wall between different pinning centers called Barkhausen volume, which is closely related to the structural properties of the material.[27] On the other hand, it was stated by Gaunt[33] that in the case of strong domain wall pinning, the volume swept between pinning centers (which in this model contains in average the volume associated with one additional pinning site) cannot be directly related to the activation volume calculated from aftereffect measurements but is inversely proportional to the density of pinning centers. Under these conditions, the Barkhausen volume can be several orders of magnitude larger than the activation volume. In some experimental studies, this distinction is clearly done by calculating the activation volume from aftereffect measurements and independently estimating the Barkhausen volume from the pinning site distribution.[34]

It is important to notice that the value of the activation volume cannot be obtained by fitting of the aftereffect measurements on long time scales. Several studies in the literature show that the value $V\Delta M/k_BT$ can be obtained from constant domain-wall velocity measurements at fields where the domain-wall motion is not yet in the viscous regime but in the thermally activated depinning regime that can be described by an Arrhenius law. Measurements of a constant domain-wall velocity as a function of the applied magnetic field in the Arrhenius regime lead to activation volumes which are in excellent agreement with values calculated from aftereffect measurements.[35] More specifically, these constant velocity measurements have been performed also in GaMnAs materials[36] obtaining the corresponding values for the activation volume V. In the cited GaMnAs work, the authors

TABLE I. Sample properties and overview of the extracted activation volumes.

Sample name	Mn concentration (%)	Curie temperature (K)	Film thickness (nm)	V_1 (10^4 nm^3)	V_2 (10^4 nm^3)
A (Rome)	2.5	53	170	(3.4 ± 0.2)	(3.7 ± 0.7)
B (Nottingham)	8	65	50	(1.5 ± 0.1)	(1.6 ± 0.4)

used nonlocal magnetotransport measurements to monitor constant domain-wall velocities at different fields. Most likely, the typical aftereffect profile present at long time scales has not been observed in Ref. 35 possibly because of both the small size of the devices used and, though still in the thermally activated depinning regime, larger magnetic fields than those used in our study.

Our values for the activation volumes obtained from the aftereffect measurements together with the magnetic and structural parameters of samples A and B are summarized in Table I. The magnitude of the activation volumes calculated in this work are comparable to results in the literature obtained by analyzing the field dependence of the constant domain-wall velocity in both compressively[36] and tensile strained[37] GaMnAs. The difference or nearly a factor of 2 in the values of the activation volumes for samples A and B, we attribute to the difference in the manganese concentration. Since the activation volume is a parameter closely related to the density of defects, a smaller activation volume is expected for a larger manganese concentration should each manganese center be considered as a point defect.

II. CONCLUSIONS

A detailed analysis of the irreversible magnetic aftereffect is presented in two different in-plane magnetized GaMnAs/GaAs samples A and B. The effect is measured using Kerr microscopy and magnetotransport and manifests itself in a drastic decrease in domain-wall velocity over time under constant magnetic field conditions below the coercivity. The experimental results of the time-dependent domain-wall velocity have been modeled considering two coexisting relaxation processes with different relaxation times describing the time dependence of the magnetization at fast and slow time scales. Two similar activation volumes of $(3.4\pm0.2)\times10^4$ and $(3.7\pm0.7)\times10^4$ nm^3 for sample A and $(1.5\pm0.1)\times10^4$ and $(1.6\pm0.4)\times10^4$ nm^3 for sample B have been obtained from the magnetic field dependence of the relaxation times τ_1 and τ_2, respectively. We show in this way that modeling the aftereffect signature could be of use for calculating activation volumes in a very low-field range. In this case, the pronounced curvature of the magnetization vs time dependence will allow for a linear approximation to obtain the domain-wall velocity vs magnetic field curve only at very short times. Therefore, in the low-field regime modeling, the aftereffect over a long measurement time (a larger set of data points) becomes a more reliable method to calculate the activation volume.

The origin of the two relaxation processes on fast and slow time scales considered in our model could be related to different length scales of the pinning centers that can impede domain-wall motion in this material. The well-known structural defects created during the GaMnAs growth such as interstitial manganese atoms, arsenic antisites, and the substitutional manganese itself can play a role in the pinning of domain walls at the nanometer scale. However, defects in the micrometer range such as surface imperfections can also greatly influence the domain-wall dynamics. Both types of pinning centers progressively reduce the mobility of the domain wall as its area grows larger. However, approximating the energies involved in these pinning events using a flat-topped distribution seems not to be the best choice considering the large difference in the length scales where these two processes take place. The approximation we propose is built by considering two distinct independent processes that occur simultaneously and is in excellent agreement with the experimental data. This close correspondence between the presented formulation and the results of the measurements may indicate a higher degree of accuracy of our biexponential relaxation model in resembling the complex scenario that is behind the magnetic aftereffect in GaMnAs.

ACKNOWLEDGMENTS

We wish to thank R. Skomski and A. Enders for helpful suggestions.

*l.herrera-diez@fkf.mpg.de

[1] H. Ohno, Science **281**, 951 (1998).
[2] D. Chiba, M. Sawicki, Y. Nishitani, Y. Nakatani, F. Matsukura, and H. Ohno, Nature (London) **455**, 515 (2008).
[3] L. Néel, J. Phys. Radium **11**, 49 (1950).
[4] H. Deng-lu, D. Zi-xia, Y. Cai-xia, and L. Qing-hua, J. Alloys Compd. **429**, 40 (2007).
[5] A. Lyberatos, R. W. Chantrell, E. R. Sterringa, and J. C. Lodder, J. Appl. Phys. **70**, 4431 (1991).
[6] G. P. Moore, J. Ferré, A. Mougin, M. Moreno, and L. Däweritz, J. Appl. Phys. **94**, 4530 (2003).
[7] L. Thevenard, L. Largeau, O. Mauguin, G. Patriarche, A. Lemaître, N. Vernier, and J. Ferré, Phys. Rev. B **73**, 195331 (2006).
[8] L. Néel, J. Phys. Radium **12**, 339 (1951).
[9] L. Néel, J. Phys. Radium **13**, 249 (1952).

[10] J. L. Snoek, Physica (Amsterdam) **5**, 663 (1938).
[11] H. Kronmüller, *Nachwirkung in Ferromagnetika* (Springer-Verlag, Berlin, New York, 1968), p. 63.
[12] H. Kronmüller, *Topics in Applied Physics: Hydrogen in Metals I* (Springer-Verlag, Berlin, New York, 1968), Chap. 11, p. 289.
[13] T. Weiers, G. Denninger, A. Koeder, W. Schoch, and A. Waag, Solid State Commun. **135**, 416 (2005).
[14] K. M. Yu, W. Walukiewicz, T. Wojtowicz, I. Kuryliszyn, X. Liu, Y. Sasaki, and J. K. Furdyna, Phys. Rev. B **65**, 201303(R) (2002).
[15] J. Mašek and F. Máca, Phys. Rev. B **69**, 165212 (2004).
[16] L. Herrera Diez, R. K. Kremer, A. Enders, M. Rössle, E. Arac, J. Honolka, K. Kern, E. Placidi, and F. Arciprete, Phys. Rev. B **78**, 155310 (2008).
[17] K. W. Edmonds, K. Y. Wang, R. P. Campion, A. C. Neumann, C. T. Foxon, B. L. Gallagher, and P. C. Main, Appl. Phys. Lett. **81**, 3010 (2002).
[18] R. P. Campion, K. W. Edmonds, L. X. Zhao, K. Y. Wang, C. T. Foxon, B. L. Gallagher, and C. R. Staddon, J. Cryst. Growth **247**, 42 (2003).
[19] I. Horcas, R. Fernández, J. M. Gómez-Rodríguez, and J. Colchero, Rev. Sci. Instrum. **78**, 013705 (2007).
[20] T. Dietl, H. Ohno, and F. Matsukura, Phys. Rev. B **63**, 195205 (2001).
[21] K. Y. Wang, M. Sawicki, K. W. Edmonds, R. P. Campion, S. Maat, C. T. Foxon, B. L. Gallagher, and T. Dietl, Phys. Rev. Lett. **95**, 217204 (2005).
[22] J. Honolka, L. Herrera Diez, R. Kremer, K. Kern, E. Placidi, and F. Arciprete, arXiv:0908.4210 (unpublished).
[23] H. X. Tang, R. K. Kawakami, D. D. Awschalom, and M. L. Roukes, Phys. Rev. Lett. **90**, 107201 (2003).
[24] N. Fujiwara, H. Tutu, and H. Fujisaka, Prog. Theor. Phys. Suppl. **161**, 181 (2006).
[25] E. P. Wohlfarth, J. Phys. F: Met. Phys. **14**, L155 (1984).
[26] G. Bayreuther, P. Bruno, G. Lugert, and C. Turtur, Phys. Rev. B **40**, 7399 (1989).
[27] A. Kirilyuk, J. Giergiel, J. Shen, and J. Kirschner, J. Magn. Magn. Mater. **159**, L27 (1996).
[28] K. Hamaya, T. Koike, T. Taniyama, T. Fujii, Y. Kitamoto, and Y. Yamazaki, Phys. Rev. B **73**, 155204 (2006).
[29] M. Sirena, L. B. Steren, and J. Guimpel, Phys. Rev. B **64**, 104409 (2001).
[30] B. Hohler and H. Schreyer, J. Phys. F: Met. Phys **12**, 857 (1982).
[31] A. Lisfi, J. C. Lodder, P. de Haan, T. Bolhuis, and F. J. G. Roesthuis, J. Magn. Magn. Mater. **193**, 258 (1999).
[32] P. J. Thompson and R. Street, J. Magn. Magn. Mater. **171**, 153 (1997).
[33] P. Gaunt, J. Appl. Phys. **59**, 4129 (1986).
[34] S.-B. Choe, D.-H. Kim, K.-S. Ryu, H.-S. Lee, and S.-C. Shin, J. Appl. Phys. **99**, 103902 (2006).
[35] M. Labrune, S. Andrieu, F. Rio, and P. Bernstein, J. Magn. Magn. Mater. **80**, 211 (1989).
[36] H. X. Tang, R. K. Kawakami, D. D. Awschalom, and M. L. Roukes, Phys. Rev. B **74**, 041310(R) (2006).
[37] A. Dourlat, V. Jeudy, L. Thevenard, A. Lemaître, and C. Gourdon, J. Supercond. Novel Magn. **20**, 453 (2007).